3.2. MODEL VALIDATION

3.2.1. SeaWiFS atmospheric correction background

Taking advantage of the fact that water absorption dominates other inherent optical properties in the near infrared (NIR), this spectral region is traditionally employed by the satellite ocean colour community for atmospheric correction (Bricaud et al 1987; Gordon et al 1994; Moore et al 1999). Using the simplified version of the water bio-optical model and ignoring the effects of whitecaps and sun glint on reflectance, the top of the atmosphere (TOA) reflectance received by the sensor in the SeaWiFS NIR bands can be expressed as follows:

$$\rho_t(765) = \rho_r(765) + \rho_a(765) + T_v(765)\frac{k \cdot bb(765)}{a(765)}; \quad (3.10)$$

$$\rho_t(865) = \rho_r(865) + \rho_a(865) + T_v(865)\frac{k \cdot bb(865)}{a(865)}, \quad (3.11)$$

where $\rho_t(\lambda)$ is total reflectance received by the sensor; $\rho_r(\lambda)$ is the reflectance resulting from multiple scattering by air molecules (Rayleigh scattering); $\rho_a(\lambda)$ is the reflectance resulting from multiple scattering by aerosols (includes the aerosol-Rayleigh interaction term); $T_v(\lambda)$ is the viewing diffuse transmittance from sea to sensor; $bb(\lambda)$ and $a(\lambda)$ are backscatter and absorption coefficients from the water column, respectively; and k is the wavelength independent conversion factor, relating inherent water optical properties to water reflectance. Following the SeaWiFS notation, the aerosol reflectance $\rho_a(765)$ can be expressed as

$$\rho_a(765) = \varepsilon_{7,8}\rho_a(865), \quad (3.12)$$

where the shape factor $\varepsilon_{7,8}$ is called epsilon and is defined as 765:865 nm ratio of aerosol reflectance. The value of $\varepsilon_{7,8}$ characterises the spectral variation of the aerosol extinction coefficient, which includes aerosol optical thickness, single scattering albedo, and aerosol scattering phase function (McClain et al 2000).

Since (i) the molecular reflectance $\rho_r(\lambda)$ can be computed accurately (Gordon et al 1988), (ii) $T_v(\lambda)$ is known from viewing geometry and choice of aerosol model (defined through $\rho_a(\lambda)$), (iii) $a(\lambda)$ at these wavelengths is due to pure seawater absorption and therefore is a tabulated value (Pope et al 1997), and (iv) parameter k is assumed to have low variability in natural waters and thus can be approximated as a constant (Kirk 1994), the above system (equations 3.10-3.11) is left with four unknowns, namely $\rho_a(865)$, $\varepsilon_{7,8}$, $bb(765)$ and $bb(865)$. Since there

are only two near infrared bands in SeaWiFS, the system in the present form is underdetermined and therefore cannot be solved analytically. Alternatively, one can introduce assumptions regarding the variables in equations 3.10-3.11 and thus reduce the number of unknowns and consequently bring the system to an analytically solvable form.

The classical "black pixel" approach assumes negligible water reflectance in NIR (Siegel et al 2000). Therefore, the closing equations under this assumption for the TOA reflectance are:

$$bb(765) = 0; \quad (3.13)$$

$$bb(865) = 0. \quad (3.14)$$

The assumption 3.13-3.14 is the backbone of the original SeaWiFS atmospheric correction algorithm (Gordon et al 1994). The system consisting of equations 3.10-3.11 and 3.13-3.14 is fully determined and can be solved algebraically for $\rho_a(765)$ and $\rho_a(865)$, or equally, for $\varepsilon_{7,8}$ and $\rho_a(865)$. These values are then used in the SeaWiFS data processing system to select an appropriate aerosol model by interpolating between the two bounding models from the predefined set of 12 aerosol models. The optical and radiative properties of the chosen model are then extrapolated from the SeaWiFS NIR bands into the visible spectrum, thus completing the atmospheric correction (see Gordon and Wang (1994) for an explanation of the procedure).

In coastal zones influenced by river discharge or sediment resuspension, the presence of various suspended sediments in surface waters translates into a strong backscatter signal in NIR. The resulting errors in aerosol type and concentration lead to an incorrect choice of aerosol type (defined through epsilon), and errors in both aerosol and water-leaving radiances progressively propagate towards the blue part of the spectrum. As a result, negative water-leaving radiances at shorter wavelengths are generated in some cases, a phenomenon well documented in coastal waters (Hu et al 2000; Ruddick et al 2000; Gohin et al 2002; Ametistova et al 2003). Overall, in coastal waters the atmospheric portion of the radiance received by the satellite ocean colour sensor cannot be separated without considering the ocean, and therefore the black pixel assumption must be abandoned.

A number of attempts to deal with the non-negligible water-leaving radiance in the NIR spectral region have been carried out within the SeaWiFS community. Initially, an iterative NIR correction scheme suitable for high chlorophyll waters was developed, which accounted for suspended sediment backscatter at these wavelengths (Siegel et al 2000). Since its implementation in the third reprocessing of SeaWiFS data in May 2000, the scheme has

helped to retrieve significantly more reasonable chlorophyll estimates in coastal waters from SeaWiFS (Patt et al 2003). However, it has still been targeted at waters where sediments co-vary with chlorophyll, in other words, case I waters. For the fourth reprocessing in July 2002, a NIR correction algorithm based on coupling the scattering of atmosphere and water in that spectral region was adopted, which was appropriate for sediment-rich waters (Patt et al 2003). However, empirical description of detritus and CDOM absorption, assumption of negligible backscatter in comparison to water absorption at 670 nm, as well as assumed wavelength-independent constant backscattering efficiency (i.e. fraction of backscatter in total scatter), hinder the use of this algorithm in regional applications. In summary, there is currently no operational atmospheric correction in the SeaWiFS processing suitable for turbid, sediment-rich waters.

Several other researchers have addressed the issue and a number of promising approaches have emerged. Moore, Aiken et al. (1999) developed an iteration scheme based on three NIR bands which estimates NIR water-leaving radiance, solving simultaneously for suspended sediments, aerosol thickness and aerosol type. This approach is employed operationally in MERIS processing (Aiken et al 2000). This solution to the NIR correction problem in coastal waters is promising but not applicable to SeaWiFS, which has fewer bands at those wavelengths.

Ruddick, Ovidio et al. (2000) developed a method that solves for aerosol radiance and water-leaving radiance simultaneously in the NIR, and successfully applied the technique to the highly scattering waters of the North Sea. Their method assumes spatial homogeneity of 765:865 nm ratios of aerosol as well as water-leaving reflectances whereby a user must manually determine a single aerosol type. In the context of the system of equations introduced above (equations 3.10-3.11), this approach translates into the following closing relationships:

$$\varepsilon_{7,8} = Const \tag{3.15}$$

$$\frac{T_v(765)\rho_w(765)}{T_v(865)\rho_w(865)} = Const \tag{3.16}$$

where $\rho_w(\lambda)$ is water reflectance (the last term in equations 3.10-3.11). The values for equations 3.15-3.16 are determined on the basis of scatter plots from in situ measurements or from default SeaWiFS values.

To address the same problem of reducing the number of unknowns in equations 3.10-3.11, Hu, Carder et al. (2000) established a technique to transfer aerosol type from the nearest clear

water to turbid pixels and demonstrated that the method is capable of producing qualitatively correct water-leaving radiances. Their closing relationships can be expressed as follows:

$$\varepsilon_{7,8} = \varepsilon^{cl}_{7,8} \quad (3.17)$$

$$bb(765) = bb(865) \quad (3.18)$$

where $\varepsilon^{cl}_{7,8}$ is the epsilon of the nearest clear waters. Assumption 3.18 is the first approximation of the water column backscatter because this parameter depends only weakly on wavelength. While potentially effective, this approach depends on the aerosol type remaining spatially constant over the studied area as well as on the accuracy of the assumption 3.18.

3.2.2. Atmospheric correction modification procedure

Due to proximity of the Herbert River, which constantly supplies adjacent coastal waters with particulate matter, the study area can be classified as potentially sediment-rich waters. As mentioned earlier, SeaWiFS standard atmospheric correction algorithms are inadequate in such environments due to turbidity associated with the river outflow.

To address the presence of oceanic signal in TOA reflectance in the NIR for subsequent retrieval of chlorophyll, suspended sediments and coloured dissolved organic matter in Lucinda waters from remote sensing data, the SeaWiFS algorithms were modified to allow for relaxation of the black pixel assumption. The approach is summarised below, while the actual procedure is outlined in Appendix 5.

For each turbid pixel the following system of equations in NIR is solved (for notations see equations 3.10-3.18):

$$\rho_t(765) - \rho_r(765) = \rho_a(765) + T_v(765)\frac{k \cdot bb(765)}{a(765)}; \quad (3.19)$$

$$\rho_t(865) - \rho_r(865) = \rho_a(865) + T_v(865)\frac{k \cdot bb(865)}{a(865)}; \quad (3.20)$$

$$\varepsilon_{7,8} = \varepsilon^{cl}_{7,8} \quad (3.21)$$

$$\frac{bb(765)}{bb(865)} = Const \quad (3.22)$$

$$T_v(\lambda) = T^{cl}_v(\lambda). \quad (3.23)$$

Here $\{\rho_t(\lambda) - \rho_r(\lambda)\}$ are Raleigh-corrected radiances, which equal aerosol radiances in the black pixel algorithm. The above system is completely defined and allows the retrieval of both water and aerosol reflectances in NIR. Bio-optical model calculations over the whole ranges of TSS and CHL (Table 2.1) resulted in variations of the ratio of backscattering coefficients in NIR between 1.13 and 1.15. Therefore, a constant value of 1.14 for relationship 3.22 was adopted. The aerosol type over turbid waters ($\varepsilon_{7,8}$ in equation 3.21) is "borrowed" from adjacent clear waters under the assumption that this parameter is invariant over the target area. In homogeneous clear waters a single aerosol type is used for the whole image (circa 50x50 km), while in case of intermixed clear-water aerosol types a weighted combination of aerosol models is applied to turbid waters. While the aerosol type is fixed, the aerosol concentration is allowed to vary over the image. The newly derived aerosol reflectances are then fed into the processing software SEADAS, and the default SeaWiFS atmospheric correction scheme with user-defined parameters is run to obtain modified NIR as well as visible water-leaving radiances.

This approach follows the nearest neighbour method of Hu, Carder et al. (2000), with the difference that the latter assumed backscatter coefficient to be wavelength-independent in NIR, while the present work relies on the bio-optical model results. Apart from qualitative assessment of the resultant water-leaving radiance changes, there has not been a thorough validation of the method (Chuanmin Hu, e-mail communication). The approach is expected to work as long as the assumption of spatial homogeneity of the ratio of aerosol reflectances at two NIR bands holds over the studied area. This assumption is based on the fact that although aerosol concentration can vary considerably over small spatial scales, the aerosol type (or equally, particle size distribution) is expected to vary only weakly across horizontal scales circa 200 km (Hu et al 2000; Ruddick et al 2000).

3.2.3. Application of modified atmospheric correction to validation stations

The modified atmospheric correction procedure described in the previous section and Appendix 5 was applied to 24 validation stations sampled on days with coinciding with SeaWiFS coverage (Figure 3.8). Retrieved atmospheric parameters for "clear" waters (as defined in Appendix 5) on validation days include the median epsilon, standard deviation of epsilon distribution, bounding pairs of SeaWiFS aerosol models, their weights and aerial fractions over each image (Table 3.3).

Date	Day of the year	Epsilon (s.d.)	Model Min	Model Max	Model weight	Image Coverage, %
13 July 2002	194	1.054 (0.03)	M70 C90	C70 M70	0.5 0.8	29 20
21 February 2003	052	1.050 (0.05)	M70 C90 C70	C70 M70 M50	0.6 0.6 0.5	20 13 13
22 October 2003	295	1.0755 (0.05)	M50	C50	0.25	24
17 February 2004	048	1.0325 (0.04)	M70	C70	0.4	42
20 February 2004	051	1.0725 (0.05)	M70	C70	0.5	16

Table 3.3. Atmospheric parameters over clear waters on validation days as determined by the SeaWiFS "black pixel" algorithm. Model weight is the fraction of minimum model in the combination of aerosol models. Image coverage corresponds to the fraction of an area in the image with a particular combination of aerosol models.

On 22 October 2003 and 17 and 20 February 2004, single pairs of aerosol models described the atmosphere over "non-turbid", or "clear", waters, with the number of pixels corresponding to these models comprising 24 %, 42 % and 16 % of the total of each daily image, respectively. Two pairs of uniformly intermixed aerosol models over clear waters on 13 July 2002 were associated with 49 % of the total number of pixels on that image. The 21 February 2003 image had a random uniform distribution of several aerosol models, which resulted in three pairs of aerosol models mixed over clear waters accounting for 46 % of the image pixels. Retrieved clear-water aerosol models included maritime (M50, M70) and coastal (C50, C70, C90) aerosol types at various humidity levels. Epsilon values of all these models fell within a range bounded by C50 model at the top (1.65 at 412 nm) and C90 model at the bottom (1.25 at 412 nm) (Figure 3.13). The SeaWiFS algorithm attributed the majority of turbid pixels to a single tropospheric model T50, which is the upper bound for all aerosol models employed by the SeaWiFS. Unless there was a strong source of highly scattering aerosols over these waters, the choice of this model by the SeaWiFS indicates that epsilon of these turbid pixels was overestimated by the standard SeaWiFS correction algorithm, which in turn confirms the presence of scattering sediments in these waters.

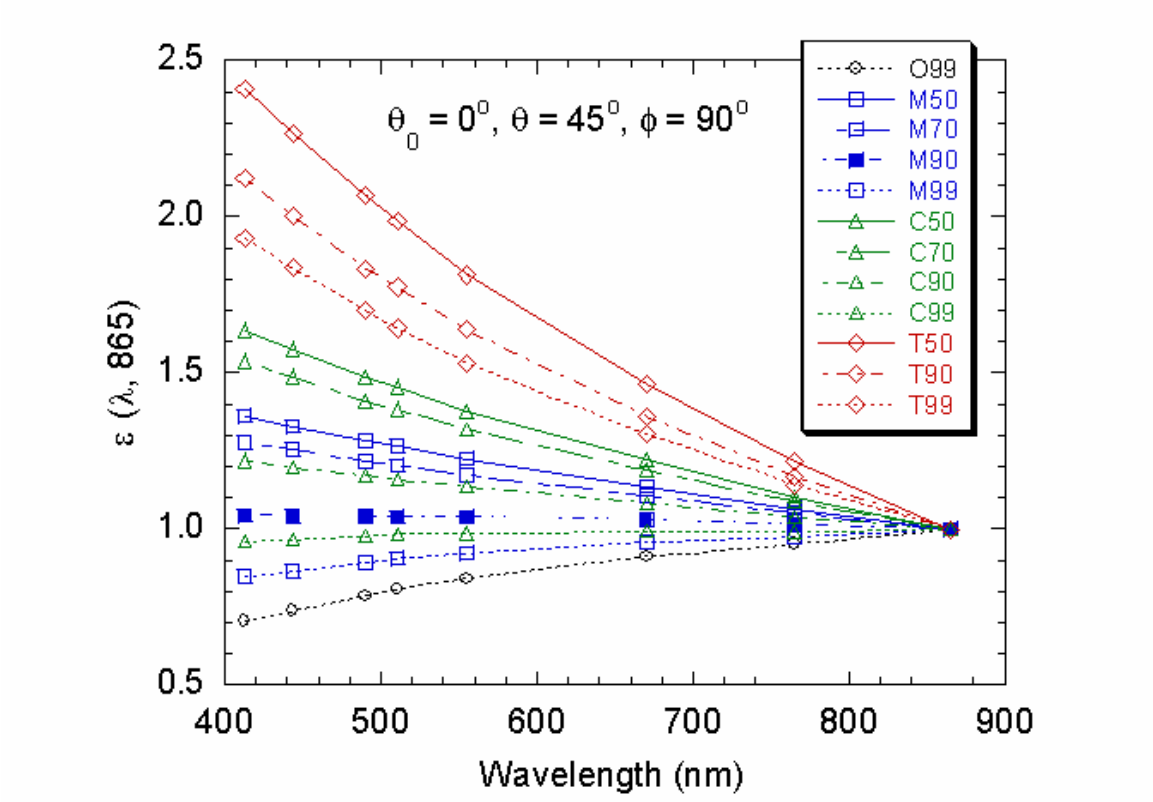

Figure 3.13. The epsilon value as a function of wavelength for the 12 aerosol models used in the current lookup tables in the SeaWiFS processing. Courtesy of Menghua Wang (Wang 2000).

The assumption of spatial homogeneity of the ratio of aerosol reflectances at two NIR bands can be tested by studying the statistical distribution of this parameter over the examined images. Standard deviations of "clear-water" epsilon values did not exceed 5 % of mean epsilon values on any of the validation days (Table 3.3), which translate into the maximum of three adjacent aerosol models that can potentially be chosen by the SeaWiFS aerosol model selection method (Figure 3.13). Extrapolation of standard deviations of epsilon to shorter wavelengths, their conversion to radiance units, and comparison with typical water-leaving radiance values in coastal Lucinda (mesotrophic scenario, Table 2.2) reveals that the application of a single aerosol type over the studied satellite images translates into variability in the water-leaving signal of about 2 % at 555 nm and 12 % at 412 nm. Since these values are close to the expected accuracy of the SeaWiFS-derived water-leaving radiances (Gross et al 2000), the aerosol type invariability within a region can be considered confirmed for validation days, and thus the proposed atmospheric correction method can be justified.

Changes in water-leaving radiance spectra derived using the modified atmospheric correction relative to their black pixel counterparts can be grouped into four types, with representative cases shown in Figure 3.14.

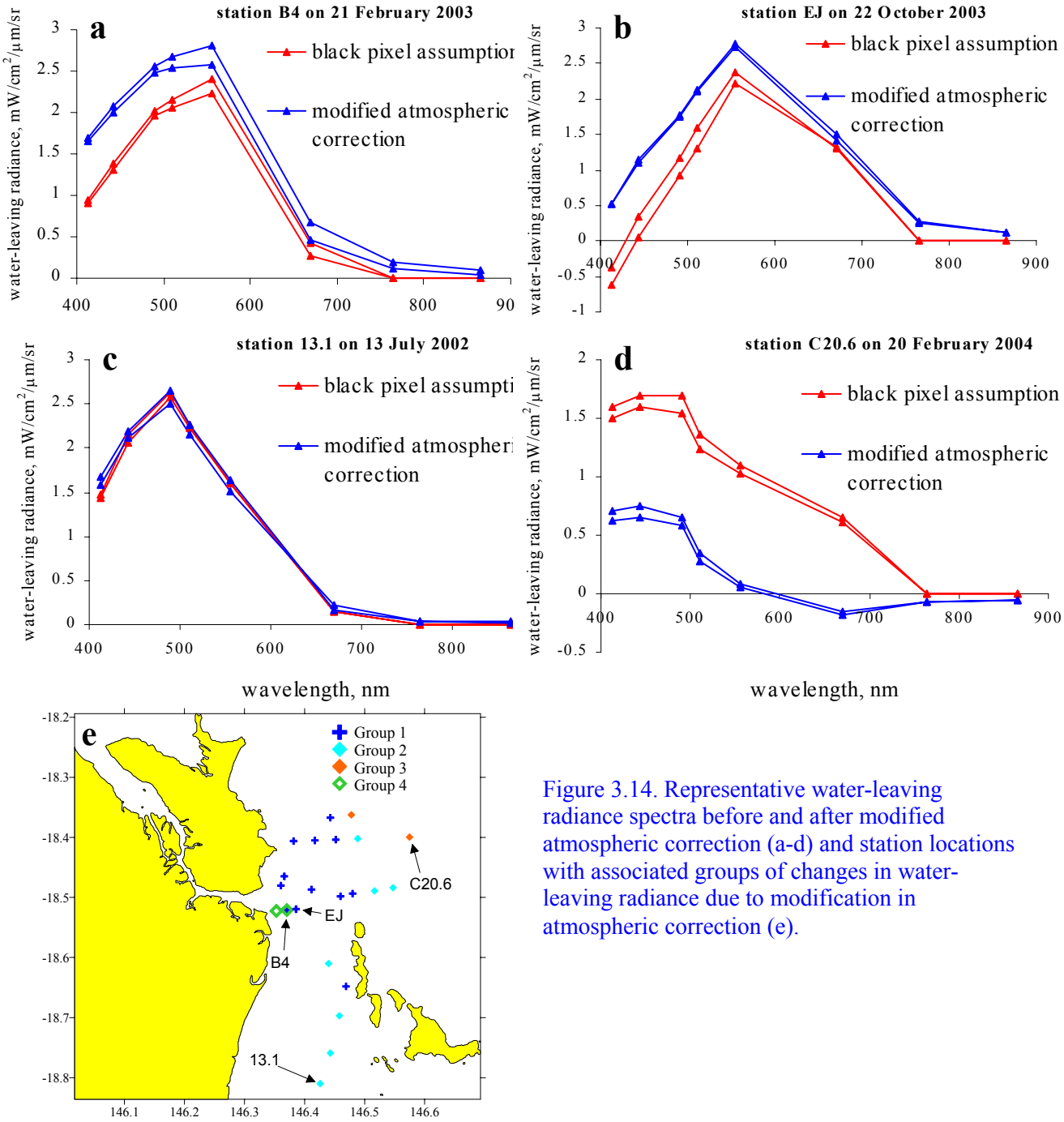

Figure 3.14. Representative water-leaving radiance spectra before and after modified atmospheric correction (a-d) and station locations with associated groups of changes in water-leaving radiance due to modification in atmospheric correction (e).

In the first group, which included the majority of the stations (13 out of 24, Figure 3.14e), the modified atmospheric correction led to gains in water-leaving radiance at all wavelengths compared to black pixel values (Figure 3.14a-b). The increase in radiance spectra indicates that by assuming a negligible ocean signal in the NIR, as with the conventional black pixel assumption, the aerosol radiance at 865 nm is overestimated, most probably due to the presence of highly scattering suspended sediments at those stations. As a result, negative water-leaving radiances at shorter wavelengths were generated in some cases (Figure 3.14b).

The modified atmospheric correction procedure eliminated this obvious inconsistency of the black pixel approach. In terms of retrieval potential, increased water-leaving radiance, such as depicted in Figure 3.14a,b, translates into a 3-fold increase in TSS, a 2-fold decrease in CDOM and a dramatic 10-20-fold increase in CHL. It should be noted that such changes are well outside the resolution of the inverse model (section 2.3.4), and therefore associated changes in water-leaving radiances produced by the modified atmospheric correction scheme are significant and cannot be attributed to noise.

For seven validation stations (Figure 3.14e), changes in water-leaving radiances resulting from the modified atmospheric correction procedure were less than the variability among adjacent pixel spectra (Figure 3.14c). In other words, the change in water-leaving radiance due to relaxation of the black pixel assumption was insignificant. All these stations are found in open-ocean waters, far from the coast and thus terrestrial sources of TSS or CDOM.

The third group consisted of two validation stations (Figure 3.14e) and was characterised by decreased water-leaving radiances relative to those with no modified NIR correction (Figure 3.14d). These stations were located in extremely clear waters close to coral reefs, where water absorption is expected to dominate the water optical signature at longer wavelengths thus resulting in essentially black waters at NIR. As a result, the modified aerosol radiance is expected to be nearly the same as the black pixel aerosol radiance. For example, at station C20.6 on 20 February 2004 the change in aerosol radiance at 865 nm produced by adopting the clear-water aerosol type was a very small positive number (0.001 $mW/cm^2/\mu m/sr$). As NIR water-leaving radiances for this station pixels are virtually zero, modified atmospheric correction procedure generated slightly negative water-leaving radiances in the last three bands and significantly lower values at other wavelengths relative to the black pixel case (Figure 3.14d). This example demonstrates that in extremely clear waters the original black pixel assumption might be a better option for atmospheric correction. Consequently, for these two stations the black pixel water-leaving radiances with zeros in NIR were used for subsequent analyses.

Finally, the two mid-jetty stations (Figure 13.4e) were classified as stray light under the black pixel assumption and therefore were not processed under the original SeaWiFS algorithm. Using the modified atmospheric correction procedure, water-leaving radiances for these pixels were retrieved.

A possible limitation of the present modified atmospheric correction procedure is the assumption that non-aerosol signal in the NIR is due explicitly to ocean sediments. At the

same time, a relatively frequent feature in SeaWiFS images is bands of "turbid" pixels around the edges of clouds. These cloud-contaminated pixels would be mistakenly taken for sediment-rich waters by the inverse bio-optical model, and thus erroneous retrievals of TSS are envisaged for such pixels. One of the possible research pathways to solve the issue could be delineating optical signatures of sediment-rich and cloud-contaminated waters. However, this is probably a task for satellite sensors with better resolved spectra, as the eight bands in the SeaWiFS are not sufficient to accommodate both water complexity and atmospheric component in the retrieval algorithms.

3.2.4. Validation analysis

SeaWiFS-derived and corrected (hereafter referred to as simply SeaWiFS- or satellite-derived) water-leaving radiances from 24 validation stations were processed by the inverse bio-optical model. The model retrieved optically significant water-colouring constituents, specifically, CHL, TSS and CDOM, and optical parameters, which included specific absorption coefficients of non-chlorophyllous and chlorophyllous particles, specific backscatter of TSS, and exponential slopes of non-CHL particles and CDOM absorption. Available in situ measurements were compared with modelled water-colouring constituents to validate the modified atmospheric correction scheme.

Water-leaving radiance

For the validation set of 24 stations the average absolute distance between the input satellite and "best-fit" modelled spectra of water-leaving radiance was 0.056 mW/cm^2/μm/sr, or equivalently, 6 % of the water-leaving radiance in the visible and 52 % in the NIR (Table 3.4). At the same time, variability of water-leaving radiance between adjacent pixels within 1.5 km of each station ranged between 12 and 88 % in the visible and NIR domains, respectively (results not shown). Therefore, the differences between modelled and observed spectra are within the stations' variability of water optical signatures.

Station	412 nm	443 nm	490 nm	510 nm	555 nm	670 nm	765 nm	865 nm	**Abs aver**
Jul02_13.1	-2.2	-0.5	2.1	-2.3	3.1	0.6	-37.0	-50.0	**12.2**
Jul02_13.2	1.6	-2.3	2.7	-2.8	4.6	10.7	200.0	150.0	**46.8**
Jul02_13.3	3.0	-0.5	2.2	-3.1	3.5	-0.8	-45.5	-58.3	**14.6**
Jul02_13.4	2.1	0.4	1.7	-2.7	4.1	18.3	27.3	0.0	**7.1**
Feb03_B2	-4.6	-3.9	1.4	-0.7	2.9	3.2	-55.4	-57.6	**16.2**
Feb03_B4	-6.4	-4.7	2.0	0.5	3.7	-16.2	-70.8	-72.9	**22.1**

Feb03_EJ	-1.8	-2.2	1.7	0.2	0.2	18.8	-28.6	0.0	**6.7**
Oct03_B4	20.3	-8.9	-3.4	-5.5	4.2	6.6	-27.7	-34.3	**13.9**
Oct03_EJ	19.9	-9.6	-1.8	-5.2	-1.5	-10.3	-45.9	-48.9	**17.9**
Oct03_Or	1.5	-2.0	2.2	-2.1	1.8	3.6	-30.8	-21.1	**8.1**
Feb04_C17.5	-2.4	1.4	1.4	-4.7	5.1	-22.2	-70.4	-72.0	**22.4**
Feb04_C17.6	-6.9	-6.2	-5.3	-6.6	7.8	-30.9	-78.8	-80.6	**27.9**
Feb04_C17.7	5.3	-9.0	-8.0	-5.9	12.2	-39.8	-87.6	-91.2	**32.4**
Feb04_C17.8	5.2	-3.9	-3.7	-2.2	11.6	-40.5	-91.7	-95.7	**31.8**
Feb04_C17.9	-14.0	-10.8	-2.9	-1.8	14.0	-37.5	-89.9	-92.4	**32.9**
Feb04_C17.10	-6.2	-5.5	-1.3	-7.4	8.3	-33.5	-83.1	-88.1	**29.2**
Feb04_C17.18	-5.2	-7.3	0.5	-4.9	3.4	8.5	-37.0	-49.7	**14.6**
Feb04_C17.19	4.6	0.6	3.5	-3.1	2.5	3.5	-13.8	-31.1	**7.8**
Feb04_C20.2	-23.2	-13.2	3.6	1.5	15.5	-19.4	-84.0	-85.9	**30.8**
Feb04_C20.3	-10.1	-11.2	1.5	-1.2	8.1	-22.4	-72.0	-74.4	**25.1**
Feb04_C20.4	-7.4	-6.4	6.3	-10.4	-12.8	-118.5	-96.8	-100.0	**44.8**
Feb04_C20.5	-1.8	-4.6	2.3	-5.4	6.0	20.0	0.0	-166.7	**25.9**
Feb04_C20.6	-9.3	-19.1	-22.9	-6.7	107.6	-106.0	-101.5	-100.0	**59.1**
Feb04_C20.J6	9.2	-1.6	-4.6	-6.3	5.2	6.6	-67.2	-58.1	**19.9**
Abs average	**7.3**	**5.7**	**3.7**	**3.9**	**10.4**	**6.2**	**55.8**	**47.7**	**23.8**

Table 3.4. Percentage distance between input satellite and "best-fit" modelled spectra of water-leaving radiance for validation stations. Absolute averages for each station and for each wavelength are provided in the last column and the last row, respectively.

Water-colouring constituents

The validation set of measured *water-colouring constituents* included TSS, which spanned between 0.01 and 12 g/m^3, CDOM with the range 0.006-0.726 m^{-1}, and CHL with the maximum measured concentration of 2 mg/m^3 and the minimum defined by the detection limit of the spectrophotometer (~ 0.27 mg/m^3). One of the optical parameters, the *exponential slope of CDOM* S_{CDOM}, was also measured in situ during field expeditions and hence was available for direct validation analysis at 17 stations.

Comparison of modelled water-colouring constituents and optical parameters with corresponding in situ measurements (Figure 3.15, note logarithmic scale for TSS, CDOM and CHL, which visually emphasises low values) reveals that TSS has the highest correlation coefficient among all water-colouring constituents, followed by CDOM, CHL and S_{CDOM} (0.89, 0.68, 0.65 and 0.60, respectively). The first three relationships are statistically significant at the 99.9 % confidence level, while the exponential slope of CDOM is statistically significant at 95 % confidence level.

While a correlation coefficient shows the degree of association between variables, it does not tell how close the regression line is to unity, i.e. how well the ground truth corresponds to satellite-derived values. To test how closely the data fitted a 1:1 line, Dr Matt Fischer (University of Sydney) graciously performed the analysis known as bootstrapping the residuals around a single weighted (the weight used was $\frac{1}{abs(y-x)}$) least squares fit for the Lucinda validation sets of water-colouring constituents (see Percival, Sardy et al. (2001) for information on "residual bootstrapping" techniques). The program used 5000 randomisations for each validation dataset, each time sampling the residuals and adding them randomly to a straight-line fit to the original data. The slopes obtained follow approximately normal distributions (Figure 3.15b,d,f,h), whereas red lines indicate the slopes that were obtained in 90 % of the 5000 randomisations (e.g. there is a 90 % chance that the slope of TSS falls between 0.43 and 1.22). Any slope that falls within the confidence interval at 90 % confidence level (i.e. within red lines) is not statistically differentiated by the available data. In other words, if the slope of a 1:1 line lies within the confidence interval, then the slope of the data is no different from a 1:1 slope, or any other slope that falls within the confidence interval. If the slope of 0 (i.e. the data are independent) lies within the confidence interval, then it is generally taken that the values are not correlated with each other.

Bootstrap confidence intervals for the slopes of the four correlations examined reveal that all validation data are correlated with their in situ counterparts, i.e. the slope 0 is outside the confidence intervals for all studied parameters (Figure 3.15). On the other hand, the slopes of unity lie within the confidence intervals for TSS, CDOM and S_{CDOM}, while for CHL the regression line of the data is statistically different from the 1:1 correspondence (the modal slope is around 0.65). Therefore, it can be concluded that satellite-derived CHL concentrations are associated with the measured values (i.e. not independent) but are not statistically equal to each other. Satellite-derived TSS, CDOM and S_{CDOM}, on the other hand, are associated and statistically correspond to measured values at the 90 % confidence level.

The model tends to overestimate chlorophyll concentrations above 1 mg/m^3, underestimate TSS above 2 g/m^3, and significantly underestimate the exponential slope of CDOM throughout the whole range of values (Figure 3.15). One of the possible causes for CHL overestimation is possible contamination of the satellite signal by chlorophyll_*a* fluorescence, which is most pronounced around 667 nm, i.e. the sixth SeaWiFS band (Roesler et al 1995; Culver et al 1997). Underestimation of CDOM exponential slope can be attributed to neglecting CDOM fluorescence in the model, especially considering the fact that all stations

with deviating S_{CDOM} were relatively CDOM-rich (CDOM absorption at 440 nm > 0.2 m^{-1}). However, there are not enough validation data to conclude that these observed tendencies are robust, and as such, more in situ and satellite comparisons are needed to support or disregard these conclusions. Overall, the validation analysis produced satisfactory results for the available data and the model can be considered validated.

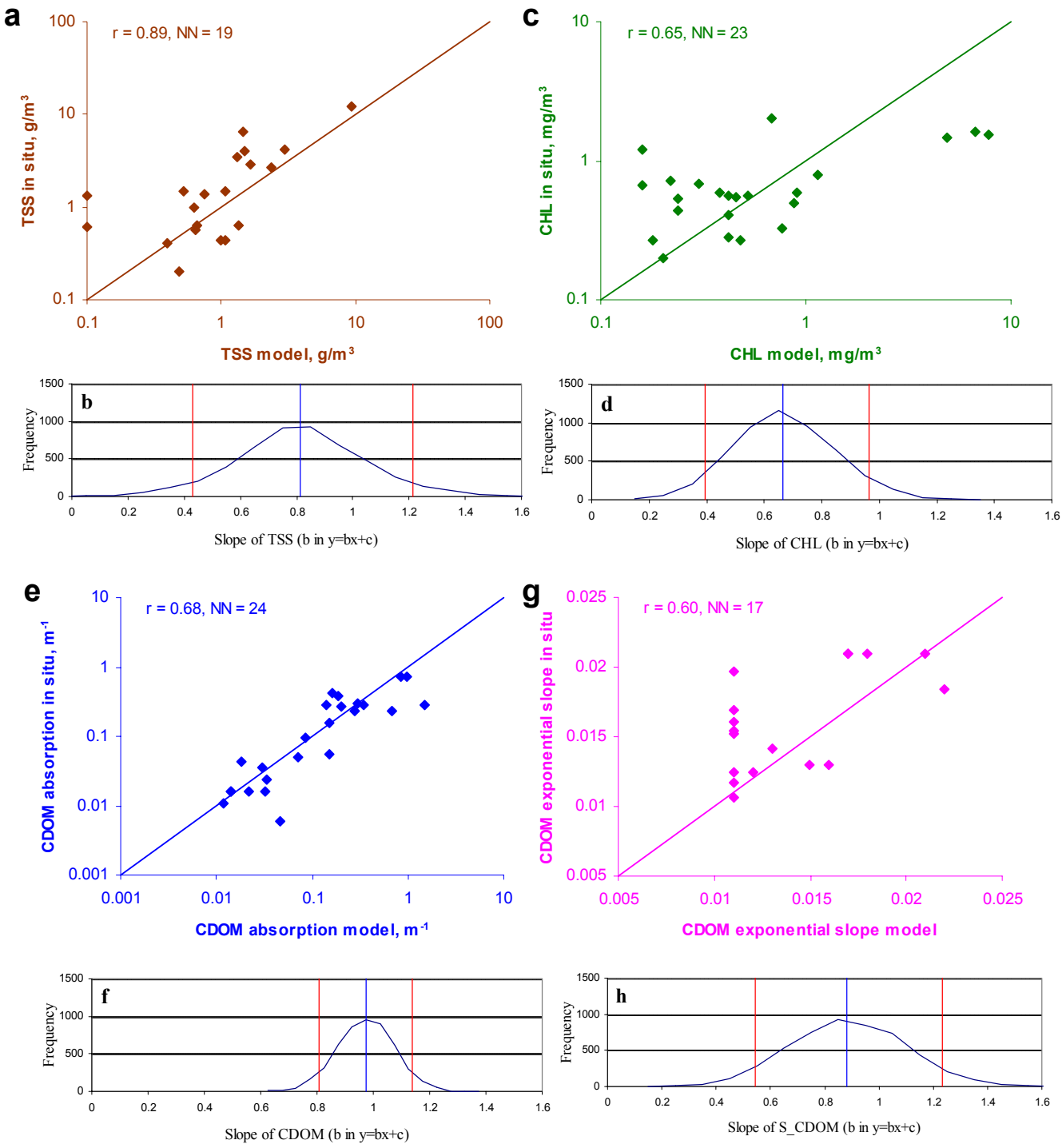

Figure 3.15. Comparison of in situ and satellite-derived TSS (a), CHL (c), CDOM absorption (e) and CDOM exponential slope (g). Values in the upper left corners show correlation coefficient r and number of validation stations NN. Slope distributions as calculated by the bootstrap of the residuals analyses are shown beneath corresponding comparisons of TSS (b), CHL (d), CDOM (f) and S_{CDOM} (h).

The present bio-optical model is capable of retrieving water-colouring constituents within a factor of two in about 80 % of the cases. The observed deviations between satellite-derived and measured values can be attributed to the following causes:

- atmospheric correction simplifications (e.g. a fixed set of standard aerosol models employed by the SeaWiFS and the assumption of spatial homogeneity of the aerosol type over the studied area);
- bio-optical model assumptions (section 2.2.8);
- measurement issues (e.g. underestimation of TSS due to neglecting particles < 0.7 μm and assumption of neutrally spectral backscatter of particles < 0.2 μm for CDOM absorption determinations);
- different spatial scales of pixel-to-point comparisons of optically significant substances. While in situ measurements refer to a point on the surface of the ocean where the sampling is undertaken, the SeaWiFS pixel is a spatially averaged (at least 1.1x1.1 km^2) value of the desired quantity. Therefore, variations of a property of interest within a pixel can lead to deviations between satellite-derived and measured values;
- time lags between satellite overpasses and in situ samplings. Although an effort was undertaken to collect validation data within the time frames recommended by the protocols for validation of ocean colour satellite products (Doerffer 2002), highly dynamic coastal regions can exhibit temporal variability on much smaller time scales.

Alternative chlorophyll parameterisation

By analysing data collected in 2002-2004 in Lucinda waters, it was found that CHL correlated strongly with CDOM in the region (Table 3.2), while CDOM optically dominated CHL at all studied sites (section 3.1.3). Therefore, as a reasonable next step, chlorophyll concentration was expressed as a linear function of CDOM absorption (the best fit regression for the available in situ data) and model validation was run with the reduced number of unknowns. This modification did not produce significant changes in TSS and CDOM retrievals, while new CHL values exhibited a much stronger relationship with their in situ counterparts, with the slope very close to unity (Figure 3.16).

These results support the definition of the optical type of Lucinda waters derived earlier (section 3.1.3), which suggests that apart from pure seawater, there are essentially two independent optically significant constituents that govern the underwater light field in the area, namely TSS and CDOM. However, this conclusion can be substantiated only within the ranges of the observed values (maximum measured CHL was 4.15 mg/m^3). Therefore,

expressing CHL through CDOM should not be extrapolated to higher values, i.e. phytoplankton bloom levels. Importantly, sensitivity analysis of the model predicts that at concentrations > 3 mg/m^3 CHL retrievals are robust under any levels of TSS and CDOM (section 2.3.2). Further validation work in the region is required for high-concentration levels of water-colouring constituents to support or reject the above finding for CHL above 3 mg/m^3.

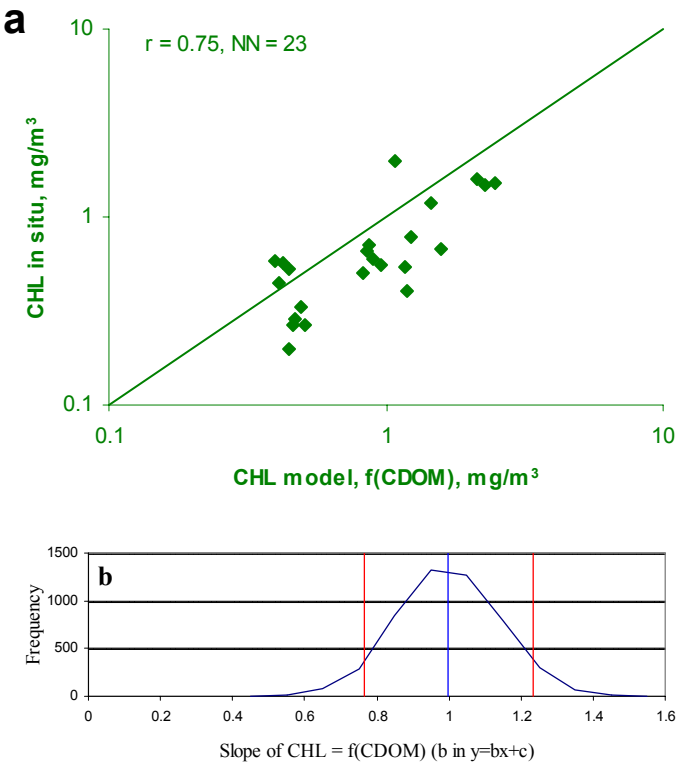

Figure 3.16. Comparison of in situ and satellite-derived chlorophyll concentrations (a) and corresponding distribution of regression slopes as derived by the bootstrap of the residuals analysis (b). Model chlorophyll is a function of CDOM.

Overall, the inverse bio-optical model generated more accurate retrievals of CHL for concentrations values below 3 mg/m^3 under the assumption of its tight relationship with CDOM. However, model sensitivity results suggest that at higher concentrations, this substance can be robustly retrieved, assuming its independence from other optically significant substances.

Model validation under alternative atmospheric correction

To test the validity of the proposed modification of the SeaWiFS atmospheric correction procedure, the model was run with water-leaving radiances derived using the original "black pixel" atmospheric correction algorithm. Results are presented in Figure 3.17. Satellite-derived "black pixel" TSS is the only water-colouring constituent, significantly (at 99 % confidence level) correlated with in situ measurements. The correlation, however, is weaker than for the modified atmospheric correction case (correlation coefficient is 0.69 as opposed

to 0.89 for the modified atmospheric correction case). Moreover, the slope of the TSS regression line is not statistically different from the unity using 90 % confidence level. CDOM as well as CHL data are not correlated (correlation coefficients are 0.36 and –0.19, respectively), indicating the absence of statistically significant associations between satellite-derived and in situ values. Overall, the modified atmospheric correction procedure resulted in much more accurate retrievals of water-colouring constituents from the SeaWiFS data than its "black pixel" counterpart. Therefore, the above results provide justification for the assumption of the spatial homogeneity of aerosol type over the studied area used in the present work.

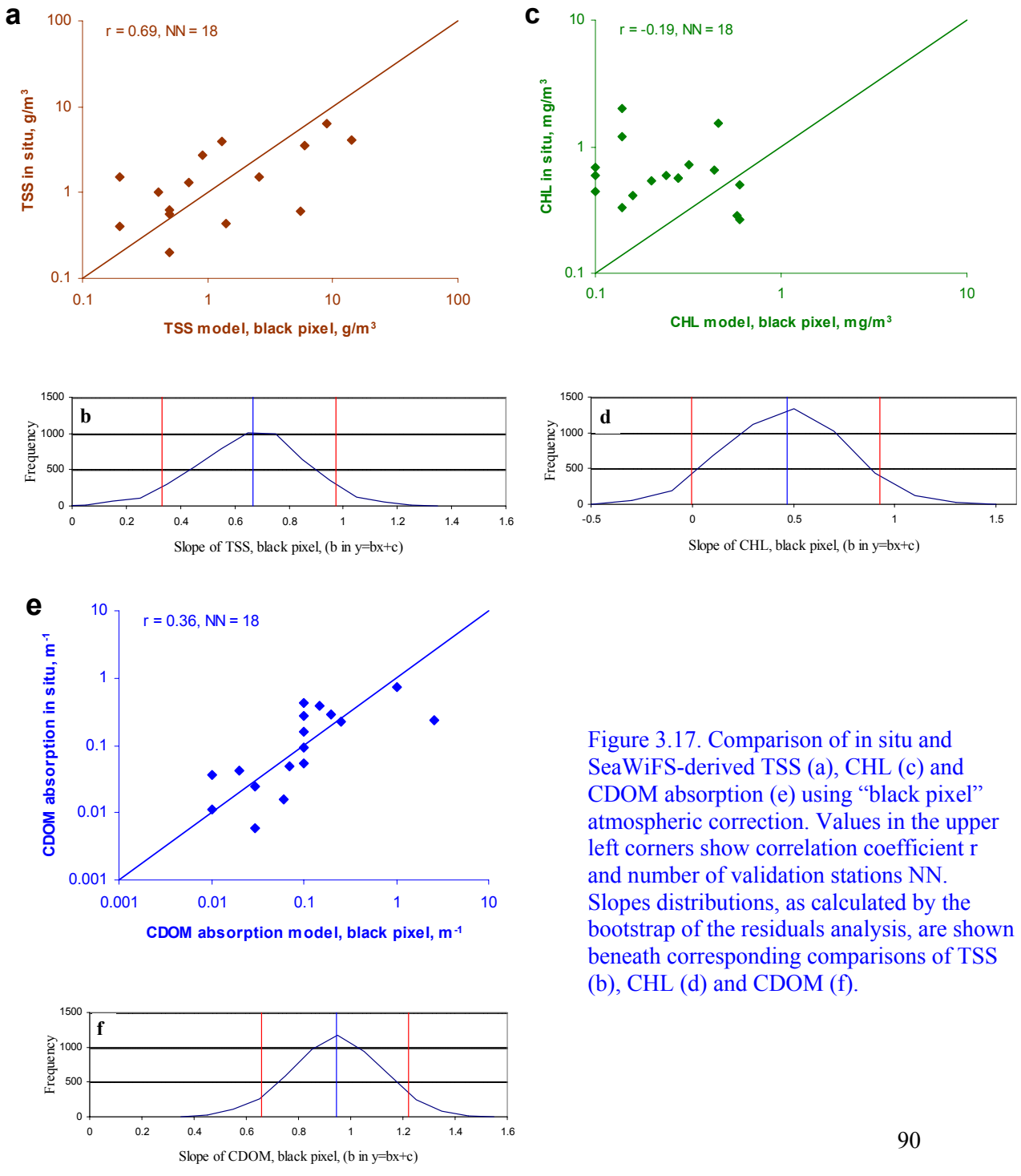

Figure 3.17. Comparison of in situ and SeaWiFS-derived TSS (a), CHL (c) and CDOM absorption (e) using "black pixel" atmospheric correction. Values in the upper left corners show correlation coefficient r and number of validation stations NN. Slopes distributions, as calculated by the bootstrap of the residuals analysis, are shown beneath corresponding comparisons of TSS (b), CHL (d) and CDOM (f).

The reason behind better TSS retrievals (relative to other constituents) using the black pixel atmospheric correction most probably lies in the fact that errors in aerosol model choice due to the black pixel assumption increase progressively towards shorter wavelengths, affecting mostly 412 nm and 443 nm (optical signatures of CDOM and CHL, respectively) and less so the 555 nm band (TSS domain). As a result, TSS can be reasonably accurately retrieved using the present bio-optical model and original SeaWiFS algorithm.

Optical parameters

It has been found by other researchers that *specific absorption coefficient of chlorophyll* is inversely related to pigment concentration in case I waters (Bricaud et al 1995, Bissett et al 1997). The packaging effect due to decreased light availability in chlorophyll-rich waters was suggested as one of the causes for the phenomena. In case II waters, on the other hand, water clarity, or equally, water turbidity, would be affected by suspended particles as well as dissolved organics. These two components are probably much more effective in blocking the light than chlorophyll per se. In coastal regions it is usually a combination of all three that tends to attenuate light in surface waters. As a result, specific absorption coefficient of chlorophyll is expected to decrease with increasing concentrations of CHL, CDOM or TSS. Indeed, the values generated by the inverse bio-optical model confirm this premise, as the low CHL-specific absorption values are found at stations with high TSS (Oct03_B4), high CDOM (Febr04_C17.6, Febr04_C17.7), and the highest among all validation stations for both TSS and CDOM (Febr04_C17.18, Febr04_C17.19) (Figure 3.18). In contrast, the high values of this optical parameter and thus smaller packaging effect are found in clear calm waters during the dry season in July 2002 and open-ocean stations in February 2004.

There is no agreement in literature on the expected variability of the *CDOM exponential slope* S_{CDOM}. On the one hand, Carder, Steward et al. (1989) observed higher slopes for predominantly fulvic acids, found mostly in freshwater humus (Visser 1984), and lower slopes for predominantly humic acids. Consequently, a decreasing offshore trend is expected. On the other hand, more researchers have found positive gradients in exponential slopes from inshore to offshore waters, which could be related to the chemical alteration of terrestrial CDOM with increasing salinity (Green et al 1994; Nelson et al 1998) as well as photochemical bleaching associated with higher availability of light in clear offshore waters (Vodacek et al 1997). Model-generated values confirm the latter hypothesis, with higher S_{CDOM} values during the sunny months of July 2002 and October 2003, as well as at post-flood offshore stations in February 2004 (Figure 3.18).

The same tendency, although not as pronounced, is observed in the modelled values of *exponential slope of non-chlorophyllous particles* (Figure 3.18). Because these particles are partly composed of degraded organisms and plants (i.e. detritus) that are subject to further bacterial decomposition, they can be considered an intermediate product in the marine trophic chain, located between living and dissolved matter. With this consideration, and keeping in mind that absorption of non-CHL particles is mainly due to detritus, CDOM is expected to have similar optical properties to those of non-CHL particulates; and similar behaviour of both types of exponential slopes is thus expected.

The general trend in organic matter content in Lucinda waters can be expressed as a smaller percentage of organic matter in waters closer to the river mouth as opposed to deeper and clearer offshore waters (Figure A10 in Appendix 4). The offshore values around unity are consistent with the case I waters definition, which suggests that all particulates in such waters are in organic form, either as CHL or detritus (Morel 1988). This observed trend agrees with the inverse correlation between organic matter content and suspended matter concentration found in most river-coastal ocean systems (Eisma 1993). As inorganic and smaller-sized particles are characterised by higher *specific backscatter coefficients of suspended matter* bb^*_{TSS} as opposed to large organic particles (Hulst 1957), higher values of bb^*_{TSS} are expected for Lucinda stations closer to the shore. Indeed, the inverse model produced a set of these optical parameters with noticeably larger values of bb^*_{TSS} for coastal validation stations, namely all jetty stations in 2003 as well as inshore stations during the last field expedition (Febr04_C17.18, Febr04_C20.J6) (Figure 3.18). The lowest specific backscatter coefficient of TSS among all 24 sites is found at the station furthest from the shore (Febr04_C20.6), in accordance with the above considerations.

The discovered tendency of organic matter content to increase in the offshore direction at Lucinda would lead to the same trend in *specific absorption of non-chlorophyllous particulates*, as large organic particles absorb much more strongly than their inorganic counterparts (Stramski et al 2001). This, however, is not the case for the model output where the values do not exhibit any obvious pattern (Figure 3.18). The random scatter of specific absorption of non-CHL particles can be attributed to the heterogeneous nature of the comprising matter, which is defined as *"particles of organic and partially mineralised matter formed from decayed plants and animals and their excretions"* (Bukata et al 1995). Consequently, this water-colouring constituent can encompass a wide array of organic and inorganic substances with diverse optical properties.

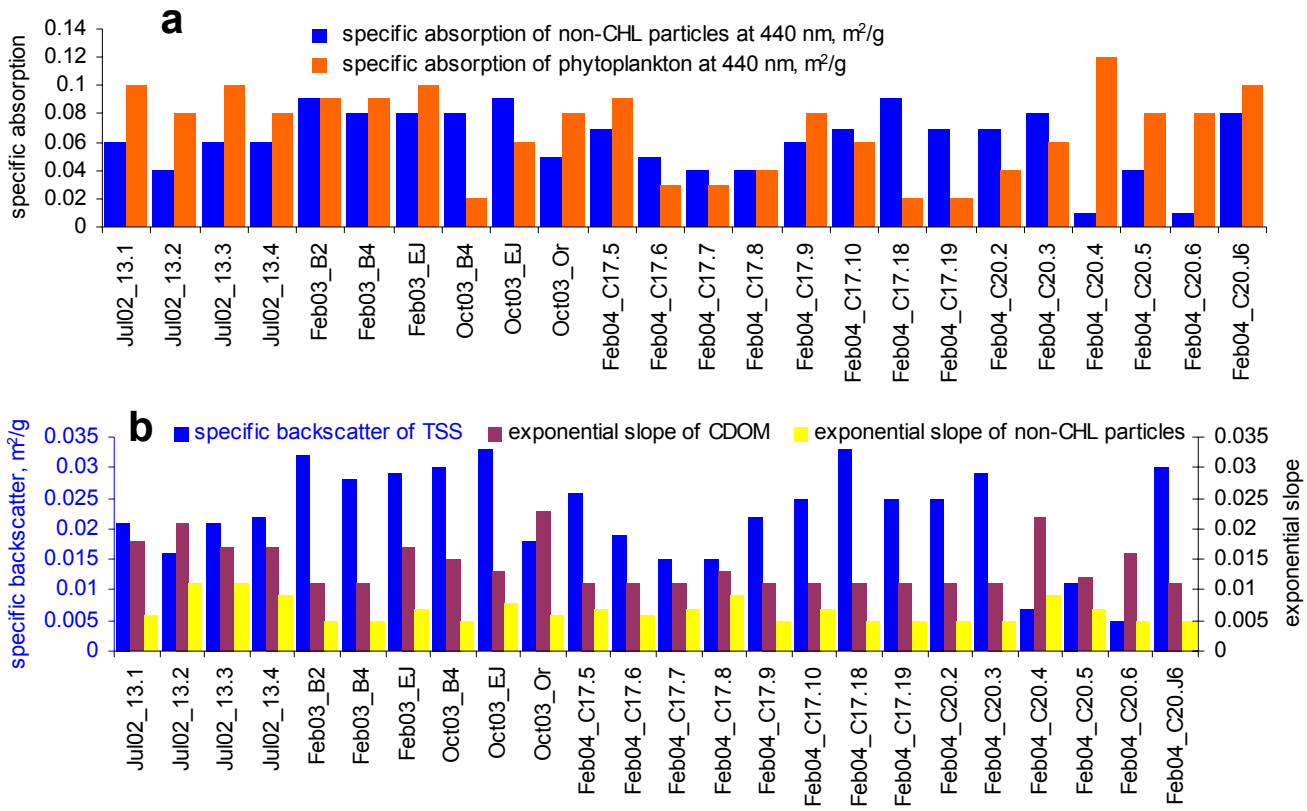

Figure 3.18. SeaWiFS-derived optical parameters of the inverse bio-optical model for 24 validation stations.

Conclusion

In summary, validation analysis of the bio-optical model developed in the present work produced encouraging results in that it was able to retrieve reasonably accurate concentrations of optically significant water-colouring constituents and physically meaningful optical parameters. To the author's knowledge, this is the first successful application of the SeaWiFS data to simultaneous retrieval and in situ validation of all three optically significant substances. The validation analysis results show that the chosen atmospheric correction procedure yielded much better retrieval of water properties than the original SeaWiFS atmospheric correction scheme. At the same time, the present model is capable of deriving reasonably accurate suspended sediment concentrations under the default SeaWiFS atmospheric processing.

Future technical improvements in sensors should result in increased spatial and temporal resolutions and better-resolved spectra. On the other hand, further developments in oceanographic and ocean optics instrumentation would provide better understanding of marine environments in optically complex coastal regions. As a result, more accurate

atmospheric correction schemes and more versatile bio-optical models that accommodate additional locally variable optical parameters are expected. At the same time, exact matches between satellite-derived and measured in situ water properties can probably never be achieved due to the previously mentioned spatial integration problem coupled with the intrinsic optical complexity of natural waters.